Microgravity Science and Technology (2020) 32:1147–1158
https://doi.org/10.1007/s12217-020-09839-3

ORIGINAL ARTICLE

Phenomenological Investigation of Drop Manipulation Using Surface Acoustic Waves

Mahdi Sheikholeslam Noori[1] · Arash Shams Taleghani[2] · Mohammad Taeibi Rahni[1,2]

Received: 9 June 2020 / Accepted: 29 September 2020 / Published online: 18 October 2020

Abstract

This paper aims at the investigation of acoustic streaming produced by surface acoustic waves (SAWs) in a drop. Computational simulation of acoustofluidic phenomenon, using lattice Boltzmann method (LBM), presenting acoustic applications in flow control, and a relatively complete parametric study are the motivations of this work. For this purpose, a computational fluid dynamics modeling based on multi-relaxation time multi-component multiphase color gradient lattice Boltzmann method was used. The simulations were carried out at wave frequencies ranging from 20 MHz to 271 MHz and wave amplitudes ranging from 0.5 nm to about 350 nm. First, the non-dimensional form of Navier-Stokes equations based on this phenomenon is presented in this work and the physics of flow is explained. Then, the consistency of the model and experimental observations is considered and our numerical results pass the physical reals. Based on our results, comparison between Lithium Niobate and Zinc Oxide Silicon devices shows that in the pumping mode, the wet length of drop on Zinc Oxide material is shorter about 10%. Also, drop moves faster on the Zinc Oxide Silicon device (about 20% in 64.5 MHz and 350 nm). Moreover, in the jetting mode, drop is detached, from Zinc Oxide Silicon device, in about 70% shorter time duration. The findings indicate that in the jetting mode a counter rotating vortex pair is formed near the drop, while the vortices are stronger for Zinc Oxide Silicon device. So, in the liquid transport applications, Zinc Oxide Silicon device is more suitable. Other important results which are presented in this work are about the non-dimensional parameters and their ranges in these phenomena. The most important non-dimensional parameters governing the physics of problem are identified. Additionally, the ranges of different physical modes (based on non-dimensional parameters) are determined, using numerical results and experimental data. The results show that in the pumping mode, Reynolds, Weber, and capillary numbers are between 3 and 1400, 10^{-5}-0.02, and 4×10^{-5}-2.5×10^{-3}, respectively. Also, in the jetting mode, the mentioned parameters are between 757 and 4600, 0.008–0.3, and 0.001–0.006, respectively.

Keywords Acoustofluidics · Surface acoustic waves · Lithium Niobate devices · Zinc oxide silicon devices · Ranges of fluidic phenomena · Phenomenological study

Introduction

Nowadays, surface acoustic waves (SAW) are one of the tools of industry and flow control and numerous devices could be found employing them on a substrate in order to achieve some specified targets. Thus far, SAWs meet the needs of many applications such as coating (Lee et al. 2019a), acoustic propeller (Tang and Kim 2019), acoustic rotary microsystems (Lu et al. 2019), pumping (Yu and Kim 2002), particle separation (Petersson et al. 2005), and mixing (Jang et al. 2007). Generally, the areas of research about SAW are presented in Ref. (Delsing et al. 2019), where the roadmap of SAWs devices is divided into three main categories as: first, quantum acoustics and single quantum systems; second, communication, sensing and actuation; and third, mesoscopic systems and collective excitations. Also, the control of fluids in microgravity is addressed in Ref. (Fernandez et al. 2017).

In this manuscript, we especially focused on the third category, i.e. drop manipulation using SAWs that leads to the field of acoustofluidics (Muller 2012). The earliest investigations about this problem were carried by Shiokawa et al. (Shiokawa et al. 1989) about 30 years ago. Also, Tan et al. (Tan et al. 2009), Brunet et al. (Brunet et al. 2010), Guo et al.

✉ Arash Shams Taleghani
Taleghani@ari.ac.ir

[1] Department of Aerospace Engineering, Sharif University of Technology, Tehran, Iran

[2] Aerospace Research Institute (Ministry of Science, Research and Technology), Tehran, Iran

(Guo et al. 2014), Aleksandrov et al. (Aleksandrov et al. 2018), and Ueno et al. (Ueno et al. 2007) conducted valuable experimental studies about these phenomena.

Furthermore, we can find some interesting works based on computational fluid dynamics on this topic in the literature. For example, Alghane et al. (Alghane et al. 2010) added the acoustic force as a source term in the governing equations and simulated the streaming mode. Besides, using similar strategy, Biroun et al. (Biroun et al. 2019) developed a model based on volume of fraction approach and simulated the dynamical behaviors of drop in different wave frequencies and amplitudes. Moreover, Riaud et al. (Riaud et al. 2017) separated the domain of solution into two subdomains, hydrodynamic field and acoustical field. Then, these subdomains of solution were coupled via acoustic streaming theory. Further, the method of separation of scales was applied with Ref. (Baltean-Carlès et al. 2019) to study the sources of streaming. Instead of streaming theory, the acoustic analogy was used in Ref. (Lee et al. 2019b).

In order to generate surface acoustic waves, the piezoelectric substrates are used in most applications. Therefore, the substrate of generation of waves is a key component in such devices. In the Rayleigh SAW mode the piezoelectric substrates such as Lithium Niobate, Aluminum Nitride (AlN), Zinc Oxide, and Lead Zirconate Titanate (PZT) are widely used (Fu et al. 2017). A comparison of these piezoelectric materials is presented in the Ref. (Fu et al. 2017). Also, AlN is more useful in film bulk acoustic resonator for biosensing applications (Wingqvist 2010; Zhang et al. 2018; Fei et al. 2018; Mirea et al. 2019). But for liquid transport and mixing, the Lithium Niobate and Zinc Oxide devices are more applicable. As another application, in Ref (Quintana-Buil et al. 2018), PZT is used to convert the electrical signal to mechanical signal in a technology to control boiling by means of acoustic waves.

For many applications, Lithium Niobate ($LiNbO_3$) has been used as a substrate of SAWs devices; because, this piezoelectric material can be applied in a vast range of frequencies and its level of wave attenuation is low (Delsing et al. 2019). But this material is relatively expensive and its manufacturing process is difficult. In another application, the substrate of Zinc Oxide Silicon (ZnO/Si) is used for SAW devices because of its advantages such as ease of material processing. The first main goal of this manuscript is comparison between these two materials concerning their effects on dynamical behaviors of a sessile drop. Note, the phenomenon (for example, the change of pumping mode to jetting mode) is independent of the materials. So, we must not expect to observe the different acoustic excitation results, when the materials are changed. However, some characteristics of dynamical behaviors (such as velocity of moving drop, generation of fluidic structures, and deformation shape of drop) are varied and we want to address them.

Moreover, investigation and analysis of fluidic phenomena based on non-dimensional parameters are so important in fluid mechanics. So, identification and definition of non-dimensional parameters governing the problem of dynamical behaviors of the sessile drop under SAWs is the second goal of this manuscript. In addition, we will try to describe the physical phenomena based on the fundamental equations of fluid mechanics.

For these purposes, we developed a multi-relaxation time multi-component multiphase color gradient lattice Boltzmann model (Gunstensen et al. 1991; Rothman and Keller 1988; Grunau et al. 1993; Leclaire et al. 2017) presented by Ba et al. (Ba et al. 2013) to model the problem. The rest of the present paper is organized as follows: In section 2, the governing equations and the numerical methods are described. Also, a definition of the problem is presented in this section. Then, the simulation of acoustofluidics is investigated in the last section of the paper and it is described both qualitatively and quantitatively. Also, for validation purposes, numerical results are compared with available experimental data.

Numerical Method

The present model has four steps, as follows:

1. Multi-relaxation-time (MRT) single phase collision, $(\Omega_i^k)^1$:

$$\left(\Omega_i^k\right)^1 = -\left(M^{-1}S\right)\left(m_i^k - m_i^{keq}\right). \tag{1}$$

2. Perturbation, $(\Omega_i^k)^2$:

$$\left(\Omega_i^k\right)^2 = \frac{A^k}{2}\left|\vec{f}\right|\left[w_i\frac{\left(\vec{c}_i.\vec{f}\right)^2}{\left|\vec{f}\right|^2} - B_i\right]. \tag{2}$$

3. Streaming:

$$f_i^k\left(\vec{x}+\vec{c}_i\delta t, t+\delta t\right) = f_i^k\left(\vec{x},t\right) + \left(\Omega_i^k\right)^1\left(f_i^k\left(\vec{x},t\right)\right) + \left(\Omega_i^k\right)^2\left(f_i^k\left(\vec{x},t\right)\right). \tag{3}$$

4. Recoloring step (Latva-Kokko and Rothman 2005):

$$f_i^R\left(\vec{x},t\right) = \frac{\rho^R}{\rho^R+\rho^B}\left(f_i'^R\left(\vec{x},t\right) + f_i'^B\left(\vec{x},t\right)\right) + \beta\frac{\rho^R\rho^B}{\rho^R+\rho^B}w_i\cos\varphi_i\left|\vec{c}_i\right|, \tag{4 - a}$$

$$f_i^B\left(\vec{x},t\right)=\frac{\rho^B}{\rho^R+\rho^B}\left(f_i'^R\left(\vec{x},t\right)+f_i'^B\left(\vec{x},t\right)\right) \quad (4-b)$$
$$-\beta\frac{\rho^R\rho^B}{\rho^R+\rho^B}w_i\cos\varphi_i\left|\vec{c}_i\right|.$$

Where, $f_i^k\left(\vec{x},t\right)$ is the total distribution function in ith velocity direction at position $\vec{x}$ and time t, subscript i is lattice velocity direction, superscript k represents the red and blue fluids (liquid or gas phases), $\vec{c}_i$ is the lattice velocity in ith direction, and δt is time step.

The particle velocity vector in a D2Q9 LBM (two dimensions and nine moments), is as follows:

$$\vec{c}_0=(0,0),\vec{c}_1=(1,0),\vec{c}_2=(0,1),\vec{c}_3=(-1,0),\vec{c}_4=(0,-1),$$
$$\vec{c}_5=(1,1),\vec{c}_6=(-1,1),\vec{c}_7=(-1,-1).\vec{c}_8=(1,-1). \quad (5)$$

M and its inverse matrix are presented in the appendix of A.1. Also, S is a diagonal matrix given by:

$$S=diag(s_0,s_1,s_2,s_3,s_4,s_5,s_6,s_7,s_8)$$
$$=diag\left(0,s_e,s_\zeta,0,s_q,0,s_q,s_v,s_v\right). \quad (6)$$

where the element s_i represents relaxation parameter. These parameters are chosen as $s_e = 1.25$, $s_\zeta = 1.14$, $s_q = 1.6$ and, s_v is related to the dynamic viscosity of two fluids and is $\frac{1}{\tau}$ where τ is the relaxation time parameter which is related to fluid viscosity (Reis and Phillips 2007). The equilibrium distribution function in the interaction mode space, m_i^{keq}, is obtained by:

$$m^{keq}=\rho^k\left(1,-3.6\alpha^k-0.4+3\left|\vec{u}\right|^2,5.4\alpha^k-1.4-3\left|\vec{u}\right|^2,u_x,\left(-1.8\alpha^k-0.2\right)u_x,u_y,\left(-1.8\alpha^k-0.2\right)u_y,{u_x}^2-{u_y}^2,u_xu_y\right)^T, \quad (7)$$

where $\vec{u}$ is flow velocity (u_x and u_y are x and y components, respectively) and it is obtained by:

$$\vec{u}=\sum\sum f_i^k\vec{c}_i. \quad (8)$$

α^k is a free parameter that the stable interface assumption requires to satisfy the following relation:

$$\frac{\rho^{R^0}}{\rho^{B^0}}=\frac{1-\alpha^B}{1-\alpha^R} \quad (9)$$

Constraint of $0\le\alpha^k\le1$ should be satisfied to avoid the unreal value of speed of sound and negative value of fluid density. Also, we can write $m_i^k=\sum_j M_{ij}{f_j}^k$. It is worth noting that to recover exact Navier-Stokes equations; we add a source term, which is recommended by Ba et al., (Ba et al. 2013), in Eq. (1).

In the perturbation operator, A_k is a parameter that affects the interfacial tension and $\vec{f}$ is the color-gradient which is calculated as:

$$\vec{f}\left(\vec{x},t\right)=\sum\vec{c}_i\left[\rho^R\left(\vec{x}+\vec{c}_i\Delta t,t\right)-\rho^B\left(\vec{x}+\vec{c}_i\Delta t,t\right)\right]. \quad (10)$$

In addition, $B_0=-\frac{4}{27}$, $B_i=\frac{2}{27}$, for i = 1, 2, 3, 4 and $B_i=\frac{5}{108}$, for i = 5, 6, 7, 8. Using these parameters, the correct term due to interfacial tension in the Navier-Stokes equations can be recovered. Weighted constants w_i are calculated as: $w_0=\frac{4}{9}, w_1=w_2=w_3=w_4=\frac{1}{9}, w_5=w_6=w_7=w_8=\frac{1}{36}$.

The following equation shows the relationship between surface tension coefficient σ and the parameter A^k:

$$\sigma=\frac{5\rho\left(A^R+A^B\right)}{6\tau} \quad (11)$$

Moreover, in Eq. (4) $f_i'^k$ is the post-perturbation value of the distribution function, φ_i is the angle between $\vec{\nabla}\rho^N$ and the lattice direction c_i, β is a parameter associated with the interface thickness and should take a value between zero and unity. Phase field, ρ^N, is defined as follows:

$$\rho^N=\left(\frac{\rho^R}{\rho^{R^0}}-\frac{\rho^B}{\rho^{B^0}}\right)/\left(\frac{\rho^R}{\rho^{R^0}}+\frac{\rho^B}{\rho^{B^0}}\right) \quad (12)$$

where ρ^{R^0} and ρ^{B^0} are the densities of the pure red and blue fluids, ρ^k is the density of each fluid:

$$\rho^k=\sum_i f_i^k \quad (13)$$

In this paper, the displacement of a two-dimensional drop affected by SAW is studied. The SAW has been modeled using a body force acting on the fluid volume. The procedure of modeling this force is explained completely in Ref. (Sheikholeslam Noori et al. 2020a), and interested readers can refer to it. This force can be computed as follows:

$$\vec{F}_{ext}^{\ k}=-\rho\left(1+{\alpha_1}^2\right)^{\frac{3}{2}}A^2\omega^2k_iexp2(k_ix+\alpha_1k_iy)\left[\sin\theta_R\vec{i}+\cos\theta_R\vec{j}\right], \quad (14)$$

where A is SAW amplitude and ω is an angular frequency which is related to SAW frequency, f, via ω = 2πf. Moreover, α_1 is attenuation coefficient, k_i is wave number, and θ_R is radiation (Rayleigh) angle. For detailed explanations about these parameters, refer to Ref. (Sheikholeslam Noori et al. 2020a).

In order to apply external body forces, the term $\overline{F}_i$ is added to Eq. (3):

$$\overline{F} = M^{-1}\left(I - \frac{1}{2}S\right)M\widetilde{F} \tag{15}$$

where I is a 9 × 9 unit matrix and $\widetilde{F}$ is as follow (Ba et al. 2013):

$$\widetilde{F}_i = w_i\left[3\left(\overrightarrow{c}_i - \overrightarrow{u}\right) + 9\left(\overrightarrow{c}_i.\overrightarrow{u}\right)\overrightarrow{c}_i\right].\overrightarrow{F} \tag{16}$$

where $\overrightarrow{F}$ is the body force.

Simulation setup is presented in Fig. 1. A drop with a certain diameter and contact angle is loaded on the substrate taken by a SAW propagating through it. Density and viscosity ratios are 1000 and 15, respectively, and surface tension coefficient is 0.072 N/m. The no-slip boundary condition is implemented on the substrate and upper side. The periodic boundary condition is applied to other sides.

In addition, the periodic boundary condition applies to the streaming step. No-slip boundary condition is applied at the solid wall by using simple bounce-back scheme (Mohamad 2011). Also, in order to simulate surface phenomena, we applied geometrical wetting boundary condition on the upper wall, which is completely described in Ref. (Sheikholeslam Noori et al. 2019).

Results and Discussions

The dynamical behaviors of a drop under SAW are depended on some different parameters which are related to physics of multi-phase flows, characteristics of an applied wave, and

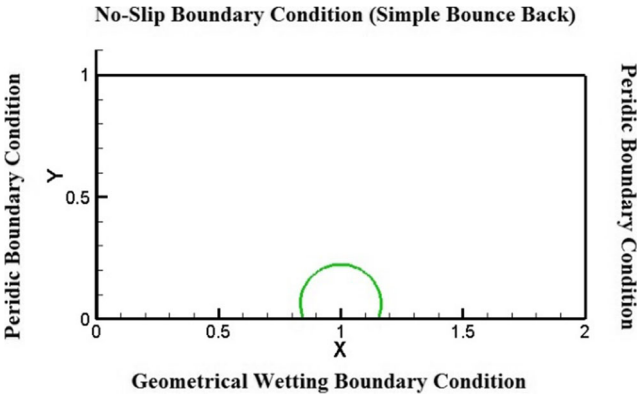

Fig. 1 Numerical domain

coupling of them. So, this applicable phenomenon is a multi-physics problem. The dynamics of drop can be classified in four modes. The first one is the streaming mode, where the drop deforms but does not move. Most experiments report that the drop deforms along the Rayleigh angle direction (Delsing et al. 2019; Fernandez et al. 2017), and internal rotational flows are observed in this mode, which are applicable in drop mixing, drop heating, particle patterning, and particle concentration.

When the applied power through SAW is increased, the drop can move steadily on the substrate, which is called the pumping mode. This mode is applicable in drop pumping in microfluidic systems, sample collecting, and sample dispensing. In the third mode, the detachment of the drop (jetting mode) is observed. Through increasing of power, the final mode which is named atomization occurs.

In the computational fluid mechanics analyses, the validation of numerical method and modeling procedure is so important. Therefore, we should firstly present some explanations for this purpose. The numerical method, which is applied in this work, is investigated in our earlier work (Sheikholeslam Noori et al. 2019) with respect to accuracy, stability, and applicability in some problems such as: stationary drop, equilibrium contact angle, drop in shear flow, and drop subjected to gravitational force.

Furthermore, the modeling of dynamical behaviors of the drop under SAW on an ideal substrate and with modeling the contact angle hysteresis is presented in the references of (Sheikholeslam Noori et al. 2020a; Sheikholeslam Noori et al. 2020b), respectively. First, we showed in these works that the numerical results are consistent with the real physics of phenomena. Second, we found that the results could be improved with considering the contact angle hysteresis about 20%. With a physical aspect, considering the contact angle hysteresis leads to modeling the real surface. For example, the roughness of the surface is considered in the simulation, and so the shape of the drop and its wetting length are simulated more accurately. Then, the boundaries of phenomena, effects of hydrophobicity, and analysis of dynamical variations of advancing and receding contact angles were investigated.

The streaming, pumping, and jetting modes are simulated and results are illustrated in Fig. 2. A traveling SAW (in the positive direction of x) with determined wave amplitude (A) and wave frequency (ω), affects a drop (which is sessile to substrate) with a certain radius (R) and contact angle (θ). In these simulations, the frequency is equal to 20 MHz. Also, the wave amplitude in the streaming, pumping, and jetting modes is 0.5 nm, 1.0 nm, and 2.0 nm, respectively. After grid resolution study, all computations are performed in 801 × 401 lattice configuration, as well.

In this section, the review of the physics based on fundamental equations of fluid mechanics, namely Navier-Stokes

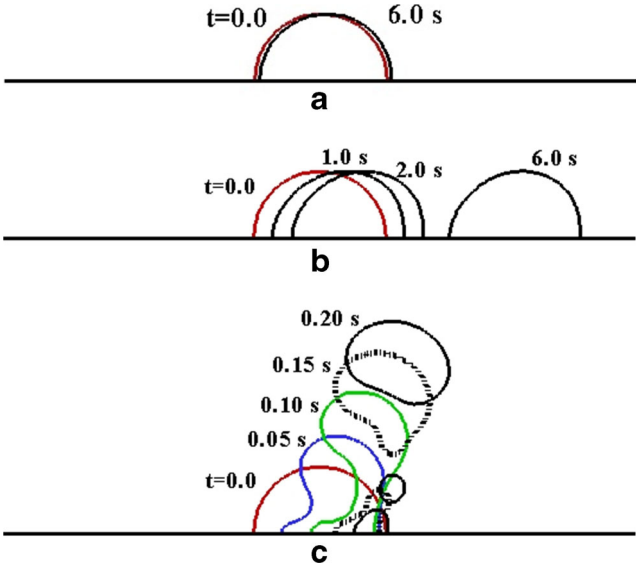

Fig. 2 Dynamical behaviors of drop under SAW. (**a**) streaming mode, (**b**) pumping mode, and (**c**) jetting mode

(N-S) equations, can be useful and interesting. In this regard, the explanations presented by Biroun et al. (Biroun et al. 2019) were very beneficial for us. The non-dimensional form of continuity and momentum equations are as follows:

$$\frac{\partial \rho}{\partial t} + \vec{\nabla}.\left(\rho \vec{u}\right) = 0, \tag{17}$$

$$\frac{\partial}{\partial t}\left(\rho \vec{u}\right) + \vec{\nabla}.\left(\rho \vec{u}\,\vec{u}\right) = -\vec{\nabla}P + \frac{1}{Re}\vec{\nabla}.\tau + \frac{1}{We}\vec{f}_{\sigma} + \frac{AR^3}{M^2}\vec{F}_{SAW} \tag{18}$$

where ρ is fluid density, $\vec{u}$ is velocity vector, P is pressure, τ is viscous stress tensor, and $\vec{f}_{\sigma}$ is surface force. Also, Re and We are Reynolds number and Weber number, respectively. These parameters are defined based on the following equations:

$$Re = \frac{\rho_L u R}{\mu_L} \tag{19}$$

$$We = \frac{\rho_L u^2 R}{\sigma} \tag{20}$$

In which, ρ_L, σ, and μ_L are density, surface tension coefficient, and viscosity of liquid, respectively and u is drop velocity. In the pumping mode, u is defined as velocity of the moving drop; whereas, u is defined as the rate of increase of the jet length before its breakup, in the jetting mode. Also, R is radius of drop. AR is wave aspect ratio which is defined as R/λ, where λ is wavelength. Also, M is similar to Mach number, where $M = u/c_s$ and c_s is the sound velocity in solid surface. It should be pointed out that gravitational force is neglected in the Eq. (2), because of micron scales. The non-dimensional form of Eqs. (1) and (2) are obtained by definition of some scaling parameters which are presented in Table 1.

Note that, F_{SAW} is a body force, which has its maximum value in receding contact angle, on the substrate, and decays exponentially in the space. This force is applied in the liquid medium. When SAW contacts with the drop, F_{SAW} generates momentum inside it. Because of viscous dissipation, the energy of SAW (which is proportional to wave amplitude and wave frequency) is transferred to the liquid medium. So, a pressure gradient in this medium is generated which forms the internal flow in the drop. The formation of internal flow leads to deformation of fluid-fluid interface and surface tension force is changed (because of variation in the gradient of the curvature of interface). This force resists against the deformation of interface and so the coupling between these forces identifies the dynamical behaviors of drop.

When F_{SAW} overcomes the inertia, the momentum inside the drop is increased and so it starts to move. In the pumping mode, surface tension force maintains the drop shape. When the energy of SAW is increased from a certain limit, the inertia of flow overcomes the surface tension and so the drop detaches from the surface.

Using the characteristics of piezoelectric surfaces is a conventional and applicable way for generation of SAW. When an alternating electric field is applied, piezoelectric crystal can be mechanically deformed (due to polarization), and so SAWs are generated on the surface of the substrate. Shiokawa et al. (Shiokawa et al. 1989), Brunet et al. (Brunet et al. 2010), and Alghane et al. (Alghane et al. 2010) used crystal of Lithium Niobate ($LiNbO_3$) as the substrate of wave propagation, while in the recent works such as Guo et al. (Guo et al. 2014) and Biroun et al. (Biroun et al. 2019), Zinc Oxide Silicon (ZnO/Si) was used. Parameters of these typical piezoelectric substrates for SAW devices are presented in Table 2.

In this section, we want to compare the dynamical behaviors of drop on these two substrates. But, at first, results must

Table 1 Scaling parameters

Parameter	Relation
Density	$\rho^* = \frac{\rho}{\rho_L}$
Time	$t^* = \frac{ut}{R}$
Space	$\vec{x}^* = \frac{\vec{x}}{R}$
Velocity	$\vec{u}^* = \frac{\vec{u}}{u}$
Pressure	$P^* = \frac{P}{\rho u^2}$
Kinematic Viscosity	$\mu^* = \frac{\mu}{\mu_L}$
Wave Amplitude	$A^* = \frac{A}{R}$
Wave Frequency	$\omega^* = \frac{\lambda\omega}{c_s}$
Wavelength	$k_i^* = \lambda k_i$

Table 2 Parameters of substrate

Parameter	$LiNbO_3$ (Alghane et al. 2010)	ZnO/Si (Biroun et al. 2019)
θ_R (°)	23	18
α_1	2.47	2.598
k_i (m^{-1})	−1340	−1813
c_s (m/s)	3485	4210

be specifically validated. Towards this end, the pumping and jetting modes when drop is attached on ZnO/Si substrate will be simulated and the obtained results will be compared with Ref. (Biroun et al. 2019). Also, after grid study, a 801 × 401 lattice configuration is used for simulations.

A drop with equilibrium contact angle, θ, of 110° is considered. SAW with A = 350 nm and f = 64.5 MHz is applied, when the wave direction is from left to right (in all simulations the wave direction is the same). Fig. 3 compares the drop shape with the experimental results (Biroun et al. 2019), while x and y coordinates relative to the center of the computational domain (x_0) are normalized by the radius of the drop. Based on this figure, maximum relative error is about 4% and we can observe that the obtained numerical results are in good agreement with reliable data.

Moreover, for validation of the jetting mode, SAW with A = 192 nm and f = 271.32 MHz is applied. Temporal evolution of drop in this mode is presented in Fig. 4 and is compared with numerical and experimental data from Ref. (Biroun et al. 2019). These results show that the dynamical behaviors of drop are modeled with acceptable accuracy.

After validation of numerical model, the dynamical behaviors of drop on different substrates are investigated and the pumping mode is firstly considered. Note that, the power of interdigital transducer which has generated the SAW, P_D, is a

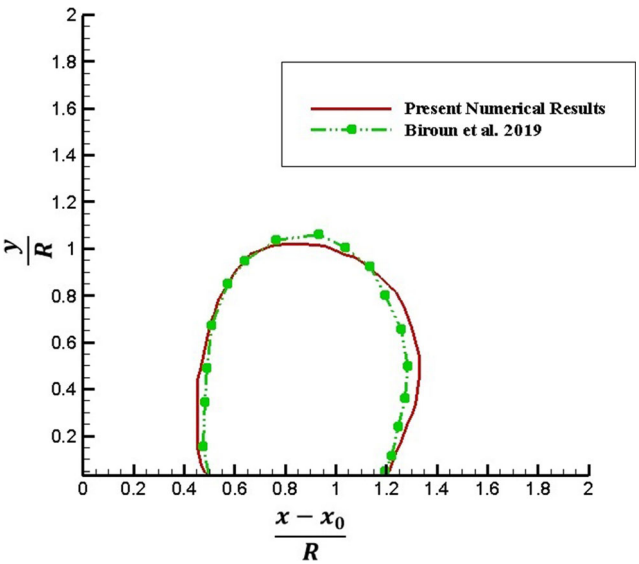

Fig. 3 Validation results: pumping mode

function of A/λ ($P_D = 8{\cdot}15 \times 10^{-6}\left(\frac{A}{\lambda}\right)^{0{\cdot}225} + 5 \times 10^{-6}\left(\frac{A}{\lambda}\right)^{0{\cdot}8}$ (Alghane et al. 2010)) and for comparisons, we applied a constant P_D (because this parameter is as the input of the device). In the previous section, SAW with f = 64.5 MHz and A = 350 nm on ZnO/Si device was considered. With respect to $f = c_s/\lambda$ and Table 2, for this situation, λ is calculated 64 μm. In constant frequency, for $LiNbO_3$ device, the wavelength is equal to 54 μm, and so for constant power situation (constant A/λ), A must be set to 295 nm. Fig. 5 compares the shapes of drop for these two devices, at the same time. Drop wet length on ZnO/Si device is shorter than $LiNbO_3$, and therefore the drop can move faster. As drop velocity on ZnO/Si device is about 160 mm/s, while drop moves on the other device with velocity of 128 mm/s.

Second, the jetting mode is considered. Additionally, the situation of SAWs with constant power is investigated. Comparable to previous results, for a wave with f = 271 MHz, the wave amplitudes on ZnO/Si and $LiNbO_3$ devices are calculated 192 nm and 154 nm, respectively. We observed that the drop was detached from ZnO/Si device faster than $LiNbO_3$ device. The drop is jetted after about 12 ms from ZnO/Si substrate, while this time duration on $LiNbO_3$ is about 20 ms (more than about 66% longer). This dynamical behavior is related to two reasons. Firstly, θ_R on ZnO/Si is smaller and so the normal component of F_{SAW}, which is responsible for detachment of drop from the substrate, is higher. Also, in a constant frequency, λ on the $LiNbO_3$ device is higher and so the wave intensity is decreased.

In addition to time duration of detachment, the dynamics of jetting is different between these devices too, and so this fact is illustrated in this section. For this purpose, in four snapshots, $t/t_0 = 0.25$, 0.5, 1.0, and 1.5, the velocity field near the substrates is presented in Fig. 5. It is worth noting that t_0 is detachment time duration (equal to 20 ms for $LiNbO_3$ device and 12 ms for ZnO/Si device). Fig. 6 shows that before jetting, two counter rotating vortices are formed near the drop, where their strengths are not equal. Also, the vortices generated around the drop are stronger for ZnO/Si device. The shapes of drop in the moment of detachment and after jetting are different between these two devices. The velocity field around the drop on ZnO/Si is more noticeable, as well.

Based on dimensional analysis, we can reach to five non-dimensional groups which are presented below. The first one is Reynolds number defined as Eq. (19). This parameter is qualitative ratio of effects of inertia to viscosity.

Second is capillary number which is defined as:

$$Ca = \frac{\mu u}{\sigma}. \tag{21}$$

Capillary number shows the ratio of viscosity to interfacial phenomena. It should be pointed out that the surface forces

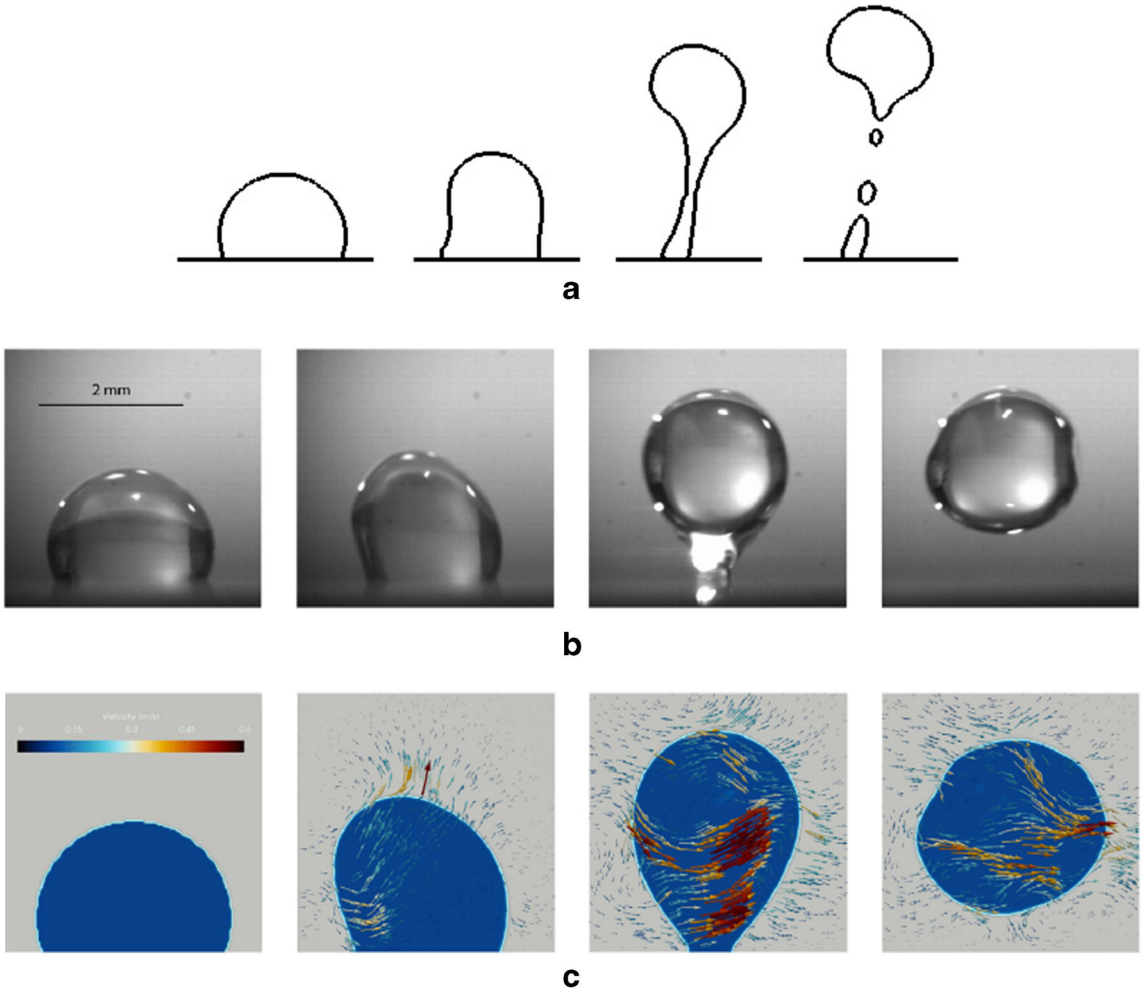

Fig. 4 Comparisons of temporal evolution of drop in the jetting mode. (**a**) present numerical results, (**b**) experimental data (Biroun et al. 2019), and (**c**) numerical results (Biroun et al. 2019)

minimize the area of the drop. Weber number is the third parameter and is the ratio of inertia to surface tension via Eq. (20). This parameter is important until it is below one and in other conditions, it can be neglected.

The Reynolds number is a general parameter and is applicable in many fluid dynamics problems. On the other hand, the capillary and Weber numbers are parameters related to physics of interfacial flows. Also, two new non-dimensional groups are specified here in order to relate the characteristics of SAW such as A and f to the fluid quantities such as ρ, μ, and σ. These two parameters are SAW amplitude and frequency numbers (Appendix A.2).

SAW amplitude number determines the effects of A and is specified as follows:

$$A_{SAW} = \frac{A\rho\sigma}{\mu^2} \tag{22}$$

A_{SAW} presents the ratio of applied surface acoustic wave force (inserted to the interface) to dissipation of momentum due to viscosity. Also, the effects of vibrations of the surface are investigated via SAW frequency number, F_{SAW}, as follows:

$$F_{SAW} = \frac{f\mu^3}{\rho\sigma^2} \tag{23}$$

First, Re as a function of A_{SAW} and F_{SAW} is presented in Fig. 7. As shown, normal axis is Reynolds number, and

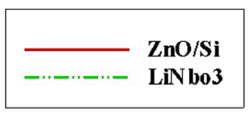

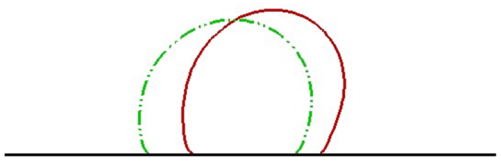

Fig. 5 Comparison of drop shape and position between ZnO/Si and $LiNbO_3$ devices

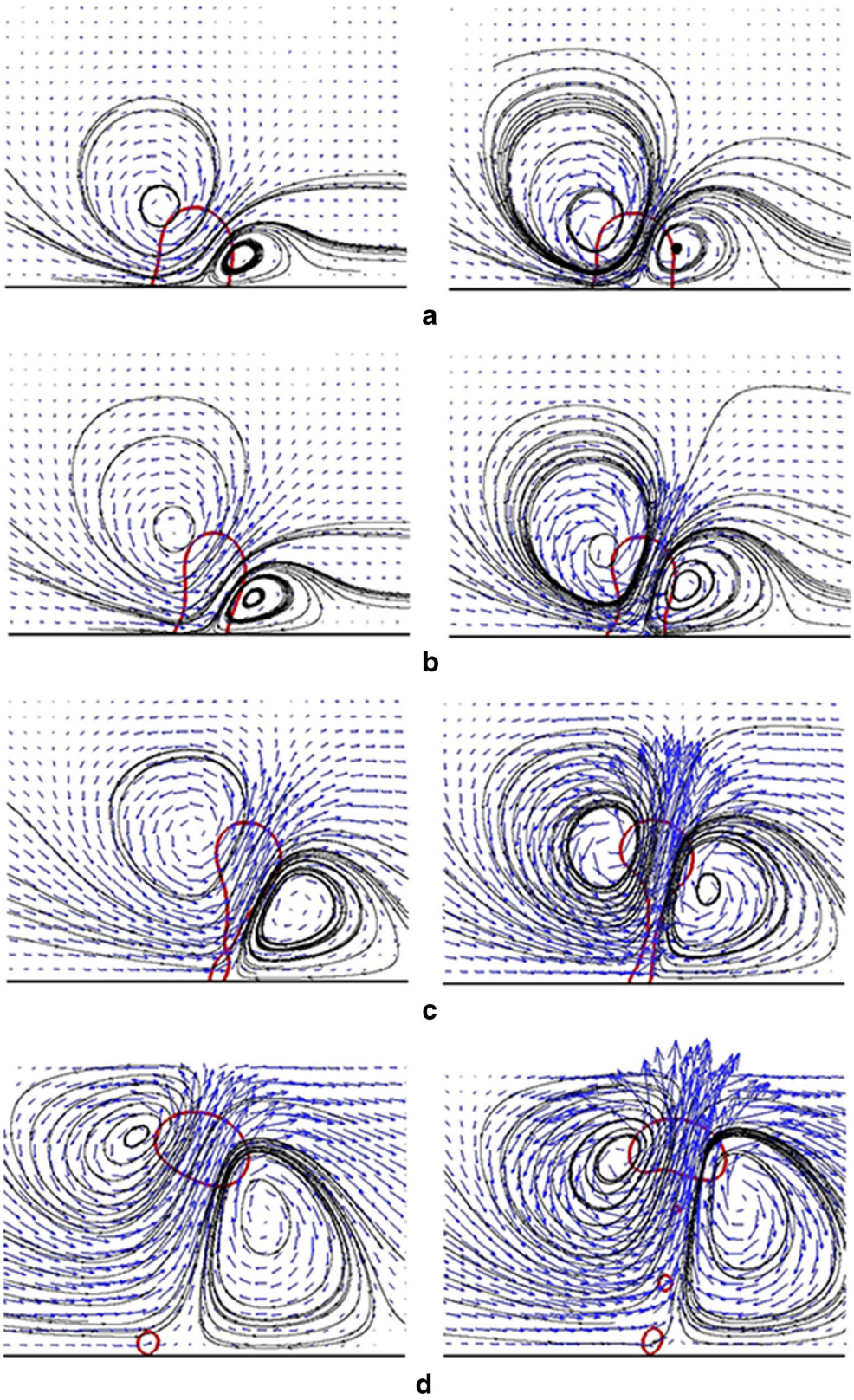

Fig. 6 Velocity field near the wall (left hand side, $LiNbO_3$ device, and right hand side, ZnO/Si device). (**a**) $t/t_0 = 0.25$, (**b**) $t/t_0 = 0.5$, **c)** $t/t_0 = 1.0$, and (**d**) t/t0 = 1.5

horizontal axis in Fig. 7-**a**, is A_{SAW} and in Fig. 7-**b** is F_{SAW}. In these figures, numerical results (obtained by our modeling and computations) are compared with about one hundred available experimental data (extracted from references (Delsing et al. 2019; Fernandez et al. 2017)), too. The square symbols relate to the pumping mode and the circle symbols represent the

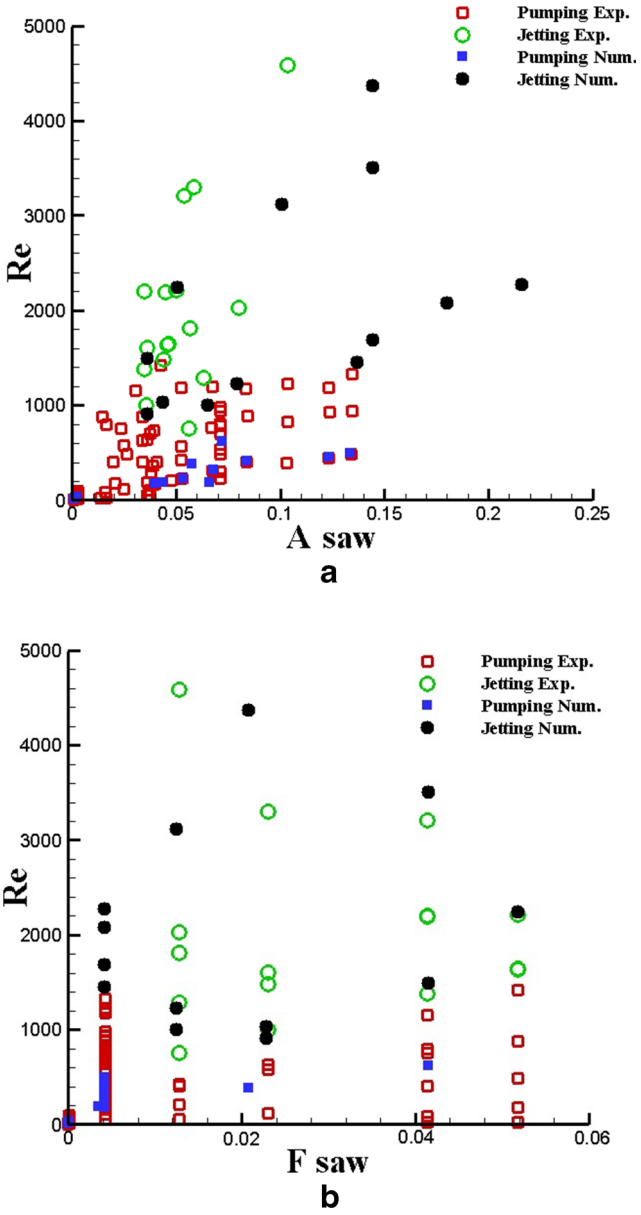

Fig. 7 Reynolds number versus characteristics of wave. (**a**) Re as a function of A_{SAW}, and (**b**) Re as a function of F_{SAW}

jetting mode. Moreover, the filled symbols are the numerical results and other ones are the experimental data. Based on these figures, an increase in A_{SAW} (in constant wave frequency) or F_{SAW} (in constant wave amplitude), is resulted in an increase in Re, accordingly. When A_{SAW} and F_{SAW} are increased, the transferred energy to the drop is increased too, and the drop with a higher velocity slides on the substrate or detaches from it. Also, we can observe that Re is in the range of 3–4600, wherein the pumping mode $3 < Re < 1400$ and in the jetting mode $757 < Re < 4600$.

Tan et al. determined the ranges of Re in the inertia dominant mode (when the size of drop is so greater than wavelength) (Tan et al. 2009). Based on their results, in the pumping and jetting modes Re is in the order of 1 and 1000, respectively. Note that they defined Re based on streaming velocity, while we defined this parameter based on velocity of the moving drop. So, the differences in the results are due to this important difference in basic calculations.

The variations of Weber number are illustrated in Fig. 8. These figures show that the importance of surface phenomena in the pumping mode is more than in the jetting mode. Also, Weber number changes from 10^{-5} to 0.3, while in the pumping mode $10^{-5} < We < 2 \times 10^{-2}$ and in the jetting mode $8 \times 10^{-3} < We < 0.3$.

The effects of variations of wave characteristics on capillary number are investigated in Fig. 9. The jetting mode occurred when the surface tension cannot remain the drop shape,

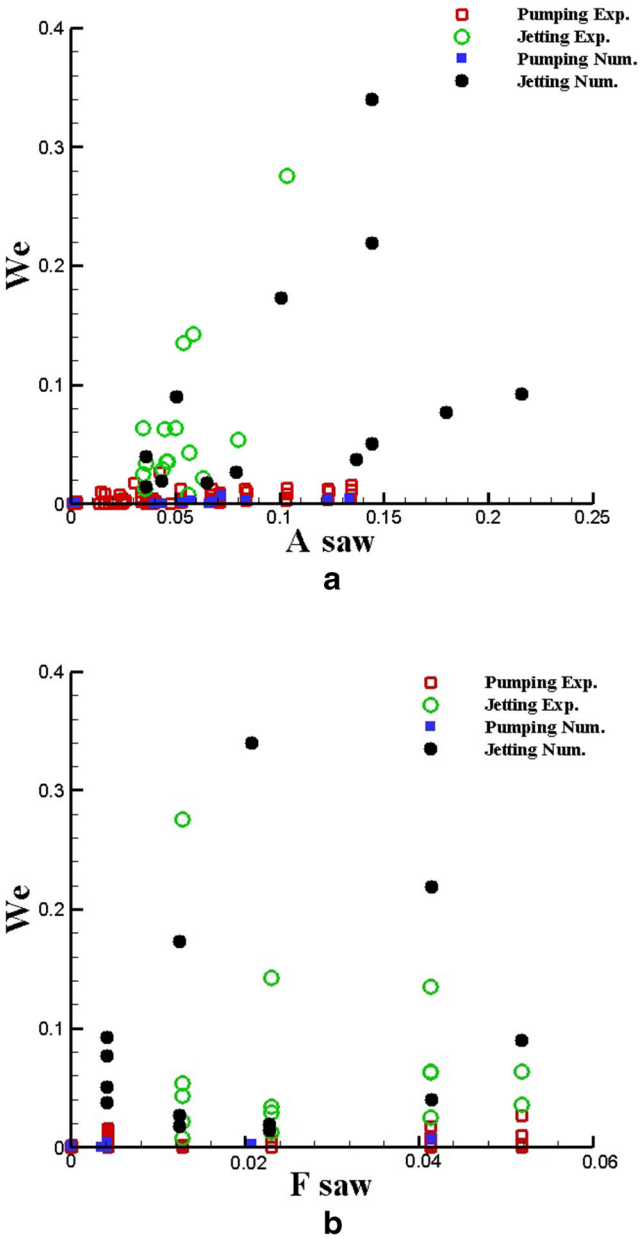

Fig. 8 Weber number versus characteristics of wave. (**a**) We as a function of A_{SAW}, and (**b**) We as a function of F_{SAW}

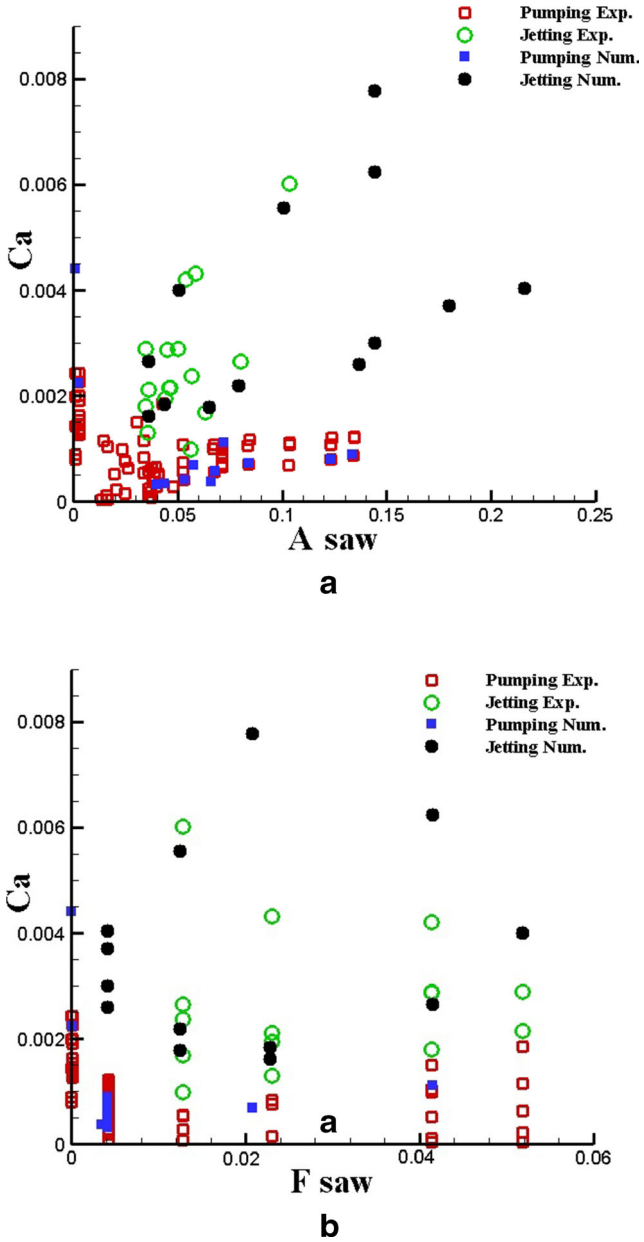

Fig. 9 Capillary number versus characteristics of wave. (**a**) Ca as a function of A_{SAW}, and (**b**) Ca as a function of F_{SAW}

and so Ca in the jetting mode is higher. Capillary number is in the range of 4×10^{-5}-2.5×10^{-3} in the pumping mode and the range of 10^{-3}-6×10^{-3} in the jetting mode.

About these three figures, there is a very important note, which is pointed here. The numerical simulations and experimental data give distinct values for the same control parameters, as it is observed in the figures. Note that, in a same control parameter (such as A_{SAW}), at a same time, we can have different frequencies, which lead to different phenomena (such as dynamical modes, velocities, and etc.). Specification of dynamical behaviors of drop affected by SAW based on dimensional analysis was our purpose of presentations of these results; consequently, our findings and experimental results are presented as integrated data.

Conclusion

In this paper, the displacement of a two-dimensional immiscible drop subjected to surface acoustic waves has been simulated by multi relaxation time color gradient model lattice Boltzmann method. The acoustic force has been implemented as an external body force.

In this paper, we followed two main goals. Firstly, the dynamical behaviors of drop in two devices were compared. The second was to present the physical phenomena based on non-dimensional parameters and to determine the ranges of these parameters in different modes of fluidic phenomena in this application.

The results showed that in the same condition (wave amplitude of about 350 nm and wave frequency of about 64 MHz) the drop moved with velocity of 160 mm/s on the Zinc Oxide Silicon device, while on the Lithium Niobate substrate this parameter was about 128 mm/s. Additionally, in the jetting mode, the drop is detached from the Zinc Oxide Silicon substrate after about 12 ms, while this time duration on Lithium Niobate substrate is about 20 ms. Moreover, the dynamics of jetting was investigated, while we observed that a counter rotating vortex pair was formed near the drop, while the vortices were stronger for Zinc Oxide Silicon device.

Then, we showed that five non-dimensional groups could be considered in this physics. These parameters are Reynolds number, Weber number, capillary number, surface acoustic wave amplitude number, and surface acoustic wave frequency number. We observed that when surface acoustic wave amplitude was increased, Reynolds number was increased as well. Also, Reynolds number ranged from 3 to 4600, whereas in the pumping mode it was in the range of 3–1400, and in the jetting mode it was in the limited area of 757–4600.

Dimensional study showed that the importance of surface phenomena in the pumping mode was more than in the jetting mode. Also, Weber number changed from 10^{-5} to 0.3, while in the pumping mode this parameter was in the range of 10^{-5}-2×10^{-2}, and in the jetting mode was in the range of 8×10^{-3}-0.3. In addition, capillary number was in the range of 4×10^{-5}-2.5×10^{-3} in the pumping mode and in the range of 10^{-3}-6×10^{-3} in the jetting mode.

Further studies and investigation of the following topics might improve and assist future research and fellow researchers. The acoustical filed was not computed in our modeling, which is recommended as a valuable and beneficial research topic. We suggest extensive computation of acoustical field in the drop. If this computation is completely performed, the effects of pressure radiation in the dynamical behaviors of drop could be investigated. Also, investigations of

effects of curvature of surface, temperature, microgravity condition, and standing waves on the dynamical behaviors of drop are among some other cases that worth further considerations. Furthermore, note that our simulations were two-dimensional, so the development of a three -dimensional model is an important recommendation to improve the work.

Appendix

A.1 Matrices which are used in MRT single phase collision operator ($(\Omega_i^k)^1$)

$$M = \begin{bmatrix} 1 & 1 & 1 & 1 & 1 & 1 & 1 & 1 & 1 \\ -4 & -1 & -1 & -1 & -1 & 2 & 2 & 2 & 2 \\ 4 & -2 & -2 & -2 & -2 & 1 & 1 & 1 & 1 \\ 0 & 1 & 0 & -1 & 0 & 1 & -1 & -1 & 1 \\ 0 & -2 & 0 & 2 & 0 & 1 & -1 & -1 & 1 \\ 0 & 0 & 1 & 0 & -1 & 1 & 1 & -1 & -1 \\ 0 & 0 & -2 & 0 & 2 & 1 & 1 & -1 & -1 \\ 0 & 1 & -1 & 1 & -1 & 0 & 0 & 0 & 0 \\ 0 & 0 & 0 & 0 & 0 & 1 & -1 & 1 & -1 \end{bmatrix} \tag{24}$$

$$M^{-1} = \frac{1}{36}\begin{bmatrix} 4 & -4 & 4 & 0 & 0 & 0 & 0 & 0 & 0 \\ 4 & -1 & -2 & 6 & -6 & 0 & 0 & 9 & 0 \\ 4 & -1 & -2 & 0 & 0 & 6 & -6 & -9 & 0 \\ 4 & -1 & -2 & -6 & 6 & 0 & 0 & 9 & 0 \\ 4 & -1 & -2 & 0 & 0 & -6 & 6 & -9 & 0 \\ 4 & 2 & 1 & 6 & 3 & 6 & 3 & 0 & 9 \\ 4 & 2 & 1 & -6 & -3 & 6 & 3 & 0 & -9 \\ 4 & 2 & 1 & -6 & -3 & -6 & -3 & 0 & 9 \\ 4 & 2 & 1 & 6 & 3 & -6 & -3 & 0 & -9 \end{bmatrix} \tag{25}$$

A.2 Non-dimensional flow control parameters

The dimensions of parameters are as follows:

$$[A]\rightarrow L, [\rho]\rightarrow ML^{-3}, [\sigma]\rightarrow MT^{-2}, [\mu]\rightarrow ML^{-1}T^{-1}, and\ [f]\rightarrow T^{-1}.$$

where, M, L, and T are units of mass, length, and time (base units), respectively. So, if we replace these parameters in Eq. (22), we can show that:

$$A_{SAW} = \frac{A\rho\sigma}{\mu^2} = \frac{L \times ML^{-3} \times MT^{-2}}{M^2L^{-2}T^{-2}} = 1 \tag{26}$$

With a similar approach, we can show that F_{SAW}, which is defined with Eq. (23), is a non-dimensional group, too.

References

Aleksandrov, V., Kopysov, S., Tonkov, L.: Vortex flows in the liquid layer and droplets on a vibrating flexible plate. Microgravity Science and Technology. **30**(1–2), 85–93 (2018 Feb 1)

Alghane, M., Chen, B.X., Fu, Y.Q., Li, Y., Luo, J.K., Walton, A.J.: Experimental and numerical investigation of acoustic streaming excited by using a surface acoustic wave device on a 128° YX-$LiNbO_3$ substrate. J. Micromech. Microeng. **21**(1), 015005 (2010 Dec 10)

Ba, Y., Liu, H., Sun, J., Zheng, R.: Color-Gradient Lattice Boltzmann Model for Simulating Droplet Motion with Contact-Angle Hysteresis. Physical Rev. E. **88**(10), 1–13 (2013)

Baltean-Carlès, D., Daru, V., Weisman, C., Tabakova, S., Bailliet, H.: An unexpected balance between outer Rayleigh streaming sources. J. Fluid Mech. **867**, 985–1011 (2019 May)

Biroun, M.H., Rahmati, M.T., Jangi, M., Tao, R., Chen, B.X., Fu, Y.Q.: Computational and experimental analysis of droplet transportation/

jetting behaviours driven by thin film surface acoustic waves. Sensors Actuators A Phys. **299**, 111624 (2019 Nov 1)

Brunet, P., Baudoin, M., Matar, O.B., Zoueshtiagh, F.: Droplet displacements and oscillations induced by ultrasonic surface acoustic waves: a quantitative study. Phys. Rev. E. **81**(3), 036315 (2010 Mar 18)

Delsing, P., Cleland, A.N., Schuetz, M.J., Knörzer, J., Giedke, G., Cirac, J.I., Srinivasan, K., Wu, M., Balram, K.C., Bäuerle, C., Meunier, T.: The 2019 surface acoustic waves roadmap. J. Phys. D. Appl. Phys. **52**(35), 353001 (2019 Jul 3)

Fei, C., Liu, X., Zhu, B., Li, D., Yang, X., Yang, Y., Zhou, Q. AlN piezoelectric thin films for energy harvesting and acoustic devices. Nano Energy. (2018)

Fernandez, J., Sánchez, P.S., Tinao, I., Porter, J., Ezquerro, J.M.: The CFVib experiment: control of fluids in microgravity with vibrations. Microgravity Science and Technology. **29**(5), 351–364 (2017 Oct 1)

Fu, Y.Q., Luo, J.K., Nguyen, N.T., Walton, A.J., Flewitt, A.J., Zu, X.T., Li, Y., McHale, G., Matthews, A., Iborra, E., Du, H.. Advances in piezoelectric thin films for acoustic biosensors, acoustofluidics and lab-on-chip applications. Prog. Mater. Sci. (2017)

Grunau, D., Chen, S., Eggert, K.: A lattice Boltzmann model for multiphase fluid flows. Phys. Fluids. **43**(4320), 1–15 (1993)

Gunstensen, A.K., Rothman, D.H., Zaleski, S., Zanetti, G.: Lattice Boltzmann Model of Immiscible Fluids. Phys. Rev. **43**(8), 4320–4327 (1991)

Guo, Y.J., Lv, H.B., Li, Y.F., He, X.L., Zhou, J., Luo, J.K., Zu, X.T., Walton, A.J., Fu, Y.Q.: High frequency microfluidic performance of $LiNbO_3$ and ZnO surface acoustic wave devices. J. Appl. Phys. **116**(2), 024501 (2014 Jul 14)

Jang, L.S., Chao, S.H., Holl, M.R., Meldrum, D.R.: Resonant mode-hoping micro-mixing. Sensors Actuators. **138**(1), 179–186 (2007)

Latva-Kokko, M., Rothman, D.H.: Diffusion properties of gradient-based lattice Boltzmann models of immiscible fluids. Phys. Rev. **71**(5), 1–7 (2005)

Leclaire, S., Parmigiani, A., Chopard, B., Latt, J.: Generalized three-dimensional lattice Boltzmann color-gradient method for immiscible two-phase pore-scale imbibition and drainage in porous media. Phys. Rev. E. **95**(3), 1–31 (2017)

Lee, Y.K., Youn, J.I., Kim, Y.J.. Modeling of the Effect of Ultrasonic Frequency and Amplitude on Acoustic Streaming. Light metals, (pp. 1573-1578). Springer, Cham (2019a)

Lee, Y.K., Youn, J.I., Hwang, J.H., Kim, J.H., Kim, Y.J., Lee, T.Y.: Modeling of the effect of ultrasonic amplitude and frequency on acoustic streaming. Jpn. J. Appl. Phys. **58**(SG), SGGD07 (2019b)

Lu, X., Zhao, K., Peng, H., Li, H., Liu, W.: Local enhanced microstreaming for controllable high-speed acoustic rotary microsystems. Physical Review Applied. **11**(4), 044064 (2019 Apr 19)

Mirea, T., Olivares, J., Clement, M., Iborra, E.. Impact of FBAR Design on its Sensitivity as in-Liquid Gravimetric Sensor. Sensors and Actuators A: Physical. (2019)

Mohamad, A.A., Lattice Boltzmann Method, springer, 1st edition, London (2011)

Muller, P.B.: Acoustofluidics in Microsystems: Investigation of Acoustic Streaming, Master Thesis. DTU Nanotech, Denmark (2012)

Petersson, F., Nilsson, A., Holm, C., Jonsson, H., Laurell, T.: Continuous separation of lipid particles from erythrocytes by means of laminar flow and acoustic standing wave forces. Lab Chip. **5**(1), 20–22 (2005)

Quintana-Buil, G., Garcia-Sabaté, A., Batlle, S., López, G., Sierra, V., Casas, O., González-Cinca, R.: A sounding rocket experiment to control boiling by means of acoustic waves. Microgravity Science and Technology. **30**(5), 731–736 (2018 Oct 1)

Reis, T., Phillips, T.N.: Lattice Boltzmann model for simulating immiscible two-phase flows. J. Phys. A: Math. Theory. **40**(3), 4033–4053 (2007)

Riaud, A., Baudoin, M., Matar, O.B., Thomas, J.L., Brunet, P.: On the influence of viscosity and caustics on acoustic streaming in sessile droplets: an experimental and a numerical study with a cost-effective method. J. Fluid Mech. **821**, 384–420 (2017)

Rothman, D.H., Keller, J.M.: Immiscible Cellular-Automaton Fluids. J. Stat. Phys. **52**(3), 1119–1127 (1988)

Sheikholeslam Noori, S.M., Taeibi, M., Shams Taleghani, S.A.: Multiple relaxation time color gradient lattice Boltzmann model for simulating contact angle in two-phase flows with high density ratio. European Physical Journal Plus. **134**(399), 1–15 (2019)

Sheikholeslam Noori, S.M., Taeibi, M., Shams Taleghani, S.A.: Numerical analysis of droplet motion over a flat solid surface due to surface acoustic waves. Using Lattice Boltzmann Method, Microgravity Science and Technology. **32**, 647–660 (2020a). https://doi.org/10.1007/s12217-020-09784-1

Sheikholeslam Noori, S.M., Taeibi, M., Shams Taleghani, S.A.: Effects of contact angle hysteresis on drop manipulation using surface acoustic waves. Theor. Comput. Fluid Dyn. **34**, 145–162 (2020b). https://doi.org/10.1007/s00162-020-00516-0

Shiokawa, S., Matsui, Y., and Ueda, T., Liquid Streaming and Droplet Formation Caused by Leaky Rayleigh Waves, Ultrasonic Symposium, Johoku, Hamamatsu, 432, Japan, (1989)

Tan, M.K., Friend, J.R., Yeo, L.Y.: Interfacial jetting phenomena induced by focused surface vibrations. Phys. Rev. Lett. **103**(2), 024501 (2009 Jul 7)

Tang, Y., Kim, E.S.. Acoustic Propeller Based on Air Jets from Acoustic Streaming. In 2019 20th international conference on solid-state sensors, actuators and microsystems & euro sensors XXXIII (TRANSDUCERS & EUROSENSORS XXXIII) Jun 23 (pp. 2068-2071). IEEE (2019)

Ueno, I., Kojo, T., Katase, S.: Shape oscillation of bubbles in a row excited by ultrasonic vibration. Microgravity Science and Technology. **19**(3–4), 157–158 (2007 Oct 1)

Wingqvist, G.: AlN-based sputter-deposited shear mode thin film bulk acoustic resonator (FBAR) for biosensor applications—a review. Surf. Coat. Technol. **205**(5), 1279–1286 (2010 Nov 25)

Yu, H. and Kim, E.S., Noninvasive Acoustic-wave Microfluidic Driver, 15th IEEE International Conference on Micro Electro Mechanical Systems, Los Angeles, USA (2002)

Zhang, Y., Luo, J., Flewitt, A.J., Cai, Z., Zhao, X.: Film bulk acoustic resonators (FBARs) as biosensors: a review. Biosens. Bioelectron. **116**, 1–15 (2018)